Thermo–Hyperelastic Tube Model: Numerical Simulation and Results

EL SAYED AHMAD Ahmad

Abstract

This report presents an academic finite-element simulation of a thermo–hyperelastic cylindrical tube subjected to transient thermal loading and time-dependent mechanical excitation. The model combines heat conduction, finite-strain hyperelasticity, and thermal expansion using a staggered solution strategy. The mechanical problem is treated quasi-statically, neglecting inertia effects. Numerical results illustrate temperature diffusion, thermal equilibrium, and the influence of thermal expansion on von Mises stress distributions. A brief convergence study supports the adequacy of the chosen mesh resolution for the qualitative objectives of the study.

1 Introduction

This document presents a thermo–hyperelastic tube model based on the finite element method for transient heat transfer and large-deformation solid mechanics. The work is of academic nature and is not intended to represent a specific real material or engineering component. The goal is to demonstrate qualitative thermo-mechanical behaviour and numerical coupling strategies.

The governing equations, constitutive assumptions, and weak formulations are detailed in a companion document (`physics.pdf`). The present report focuses on geometry, boundary conditions, numerical implementation, convergence behaviour, and interpretation of simulation results obtained using a FEniCSx implementation.

2 Geometry and Boundary Conditions

2.1 Computational domain

The computational domain $\Omega \subset \mathbb{R}^3$ is a cylindrical tube of length L and outer radius R. In the simulations reported here, the tube is solid (no inner cavity).

The boundary of the domain is decomposed as

$$\partial\Omega = \Gamma_{\text{top}} \cup \Gamma_{\text{bottom}} \cup \Gamma_{\text{lat}}.$$

2.2 Mechanical boundary conditions

The top face of the tube is fully fixed:

$$\mathbf{u} = \mathbf{0} \quad \text{on } \Gamma_{\text{top}}.$$

The bottom axial displacement is composed of two components:

- a slowly applied mean displacement (preload) with amplitude A_0, applied through a linear ramp during the initial time interval $t < t_{\text{ramp}}$,

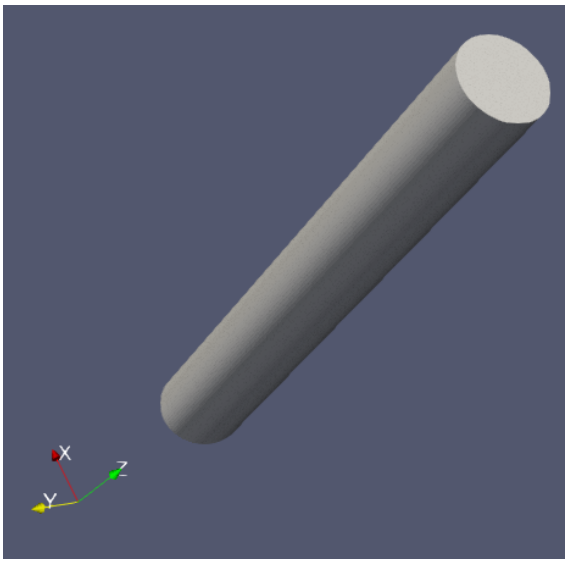

Figure 1: Schematic representation of the cylindrical tube geometry.

- a superposed sinusoidal oscillation with amplitude A, applied after the ramp phase.

Mathematically, the displacement in the z-direction is:

$$u_z(t) = \begin{cases} -A_0 \dfrac{t}{t_{\text{ramp}}}, & t < t_{\text{ramp}}, \\ -A_0 - A \sin(\omega(t - t_{\text{ramp}})), & t \geq t_{\text{ramp}}. \end{cases}$$

Because the mechanical problem is treated quasi-statically (inertia neglected), the oscillatory displacement represents a sequence of equilibrium configurations rather than a true dynamic vibration. All remaining boundaries are traction-free.

2.3 Thermal boundary conditions

A time-dependent temperature is imposed on the top face:

$$T = T_{\text{top}}(t) \quad \text{on } \Gamma_{\text{top}}.$$

Convective heat exchange is applied at the bottom face:

$$-k\nabla T \cdot \mathbf{n} = h\,(T - T_\infty(t)) \quad \text{on } \Gamma_{\text{bottom}}.$$

The lateral surface is assumed thermally insulated.

3 Finite Element Discretisation

The spatial discretisation uses linear Lagrange finite elements on tetrahedral meshes:

- Temperature: $T_h \in \mathbb{P}_1(\Omega)$,
- Displacement: $\mathbf{u}_h \in [\mathbb{P}_1(\Omega)]^3$.

Time integration of the heat equation is performed using a backward Euler scheme with constant time step Δt.

4 Material Parameters

Nominal material and model parameters used in the simulations are listed in Table 1. The values shown are representative placeholders and may be adjusted for specific simulation runs.

Table 1: Material and model parameters (nominal values).

Quantity	Symbol	Value
Young's modulus	E	$1.0 \times 10^7\,\mathrm{Pa}$
Poisson ratio	ν	0.49
Thermal expansion	α	$1.2 \times 10^{-4}\,\mathrm{K}^{-1}$
Density	ρ	$1250\,\mathrm{kg\ m}^{-3}$
Heat capacity	c_p	$1500\,\mathrm{J\ kg}^{-1}\mathrm{K}^{-1}$
Thermal conductivity	k	$200\,\mathrm{W\ m}^{-1}\mathrm{K}^{-1}$
Convective coefficient	h	$100\,\mathrm{W\ m}^{-2}\mathrm{K}^{-1}$

5 Solution Strategy and Model Assumptions

A staggered (partitioned) solution strategy is employed. At each time step, the transient heat equation is solved first. The resulting temperature field is then used to update the thermal part of the deformation gradient in the mechanical problem.

The coupling is therefore one-way:

$$T^{n+1} \longrightarrow F_{\mathrm{th}}(T^{n+1}) \longrightarrow \mathbf{u}^{n+1}.$$

Mechanical deformation does not influence the thermal problem.

5.1 Quasi-static mechanical assumption

Although the mechanical loading is time-dependent, inertia terms are neglected in the momentum balance. The mechanical problem is therefore solved quasi-statically, and each time step represents an equilibrium configuration corresponding to the current thermal state and prescribed displacement.

As a result, the model does not capture true structural dynamics, wave propagation, or inertial effects. This simplification is intentional and appropriate for the academic objectives of the study.

6 Results

6.1 Convergence at final time

A basic convergence assessment was performed by comparing results obtained on two mesh resolutions at the final simulation time. Table 2 reports representative values of temperature and von Mises stress evaluated at the tube centre.

The temperature is essentially mesh-independent, while the von Mises stress exhibits a difference of approximately one percent. This behaviour is expected, as stress is a derived quantity involving spatial gradients of displacement and converges more slowly than primary fields when using linear elements. Given the academic nature of the study, the finer mesh is deemed sufficient.

Table 2: Final-time centre values for two mesh resolutions (illustrative values).

Mesh	T_{center} [K]	$\sigma_{\text{vm,center}}$ [Pa]
Fine	332.30	1.039×10^7
Finer	332.31	1.029×10^7

6.2 Temperature distribution

Representative temperature snapshots show a smooth spatial distribution governed by diffusion and convection. After the initial thermal ramp, the temperature increases but the total time chosen is insufficient to reach full thermal equilibrium (calculations takes too long).

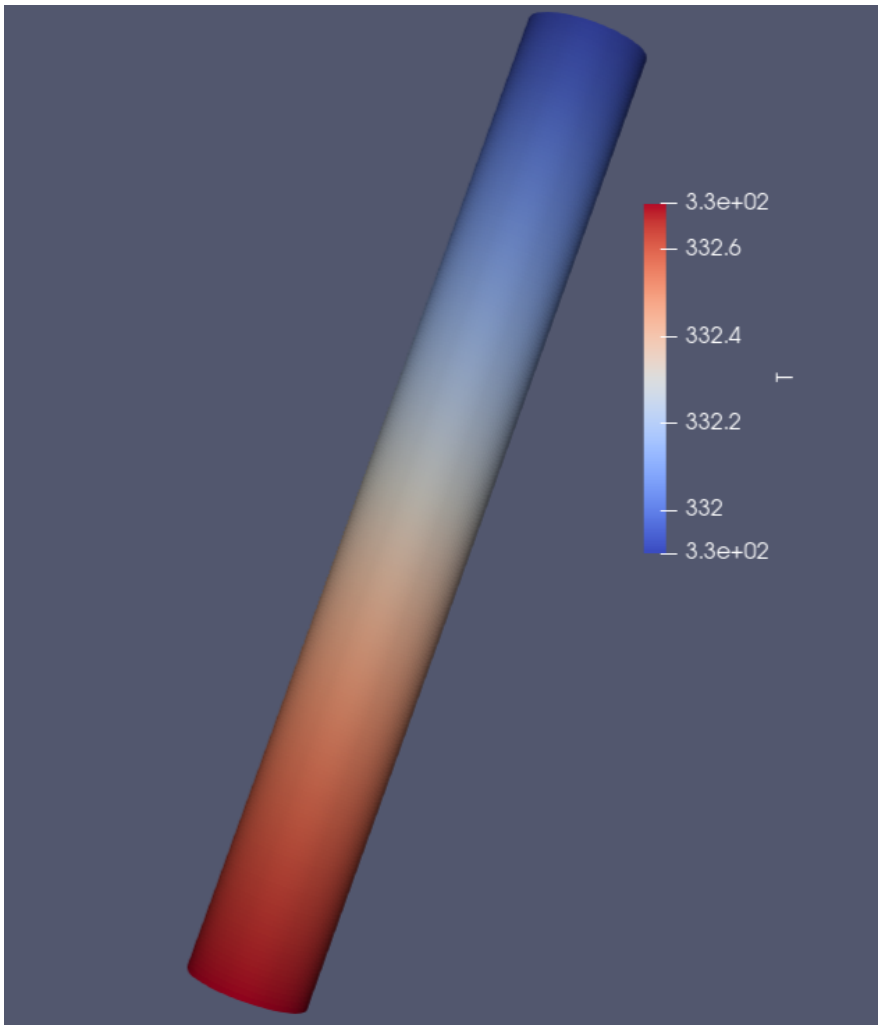

Figure 2: Temperature distribution at the last time instant (3.2 s).

6.3 Time evolution at the tube centre

Time histories of temperature and von Mises stress evaluated at the tube centre highlight the influence of thermal loading on mechanical response. As the temperature increases, the stress

adjusts accordingly due to thermoelastic coupling.

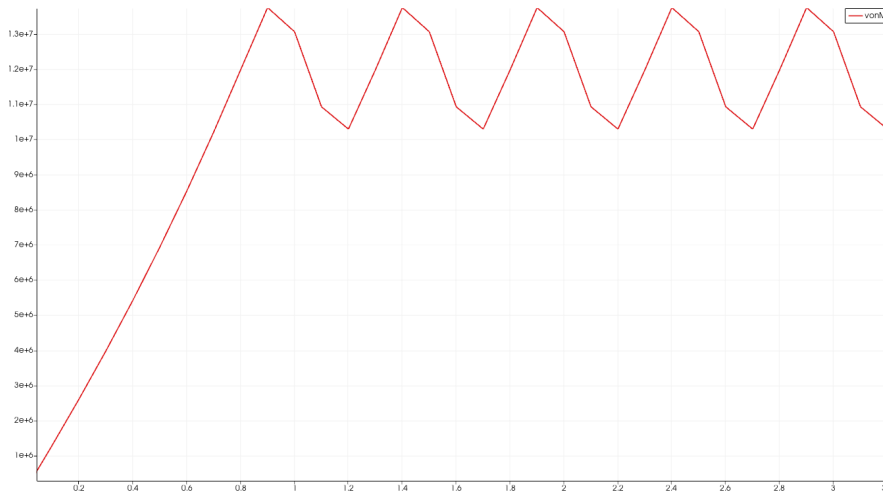

Figure 3: Time evolution of von Mises stress at the tube centre.

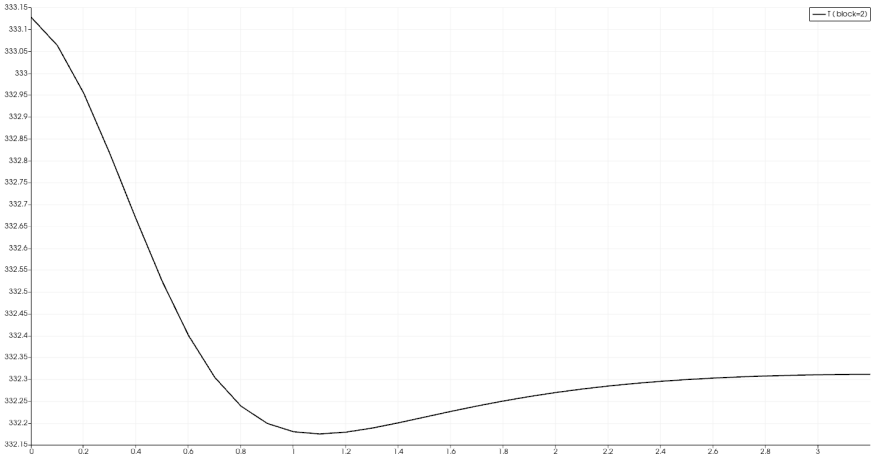

Figure 4: Time evolution of temperature at the tube centre.

7 Discussion and Limitations

The results demonstrate qualitatively consistent thermoelastic behaviour. However, several limitations must be noted. The mechanical response is quasi-static, and inertial effects are neglected. In addition, the thermo-mechanical coupling is one-way, with no feedback from deformation to the thermal problem.

These assumptions restrict the interpretation of the results to equilibrium configurations influenced by temperature evolution, but they allow a clear and robust analysis of thermal expansion effects in a finite-strain hyperelastic setting.

8 Conclusions

An academic thermo–hyperelastic tube model has been implemented and analysed using the finite element method. The staggered solution strategy captures the influence of transient temperature fields on nonlinear elastic response through thermal expansion while maintaining numerical robustness. A limited convergence study indicates that the chosen mesh resolution is sufficient for the qualitative and quantitative objectives of the study.

The framework provides a clear basis for future extensions, such as fully coupled thermo-mechanics, inclusion of inertial effects, or higher-order finite elements.